IEEE Access
Multidisciplinary | Rapid Review | Open Access Journal

Received May 17, 2017, accepted July 24, 2017, date of publication August 11, 2017, date of current version September 6, 2017.

Digital Object Identifier 10.1109/ACCESS.2017.2737326

Reducing the Impact of Thin Clouds on Arctic Ocean Sea Ice Concentration From FengYun-3 MERSI Data Single Cavity

XING-DONG WANG[1,2,3], ZHAN-KAI WU[1], CHENG WANG[1], XIN-WU LI[2], XIN-GUANG LI[1], AND YU-BAO QIU[2]

[1]College of Information Science and Engineering, Henan University of Technology, Zhengzhou 450001, China
[2]Institute of Remote Sensing and Digital Earth, Chinese Academy of Sciences, Beijing 100094, China
[3]Key Laboratory of OptoElectronic Science and Technology for Medicine of Ministry of Education, Fujian Provincial Key Laboratory of Photonics Technology, Fujian Normal University, Fuzhou 350007, China

Corresponding author: Xing-Dong Wang (zkywxd@163.com)

This work was supported in part by the National Natural Science Foundation of China under Grant 41606209, in part by the National Key Research and Development Program of China under Grant 2016YFB0501501, in part by the Fujian Provincial Key Laboratory of Photonics Technology, Key Laboratory of Optoelectronic Science and Technology for Medicine of Ministry of Education, Fujian Normal University, China, under Grant JYG1707, in part by the Polar Science Strategic Research Foundation of China under Grant 20150312, in part by the Fundamental Research Funds for the Henan Provincial Colleges and Universities under Grant 2015QNJH16, in part by the Science and Technology Project of Zhengzhou Science and Technology Bureau under Grant 20150251, and in part by the High-Level Talent Scientific Research Fund Item of Henan University of Technology under Grant 150525.

ABSTRACT Arctic sea ice concentration information can provide technical support for the safety of Arctic shipping routes using visible and near-infrared satellite imagery, but clouds reduce detection accuracy. According to the reflectance changes of ice, clouds, and water, and because the near-infrared reflectances of clouds are much higher than that of ice and water, we propose a new method for identifying clouds. On this basis, thin clouds are extracted using atmospheric precipitation. The Arctic Ocean sea ice distribution under thin cloud cover over can be obtained based on the proposed influential factor iteration method. Finally, we obtain the sea ice concentration in the critical region of Baffin Bay and Davis Strait on June 15, 2014 from the Medium Resolution Imaging Spectrometer (MERSI) data. MERSI is one of the major payloads of the Chinese second-generation polar-orbiting meteorological satellite, FengYun-3, and is similar to the Moderate-resolution Imaging Spectroradiometer. The proposed method is shown to accurately detect sea ice concentration under thin clouds by comparison with the sea ice results from the National Snow and Ice Data Center.

INDEX TERMS Sea ice concentration, FengYun-3 satellite, thin clouds, atmospheric precipitation, influential factor iteration method.

I. INTRODUCTION

The Arctic is an important component of the global climate system, and also an indicator of global climate change [1]–[3]. The atmosphere, ocean, and sea ice directly or indirectly affect the strength of global atmospheric circulation, heat balance and climate change. Both ice sheets and sea ice, with high albedo, are key factors that affect the global climate system [4], [5]. In recent decades, Arctic sea ice has been shrinking and thinning year to year, due to the effects of global warming. As a consequence, the Arctic Passage is navigable in summer, which allows ships to sail the Arctic Passage, connecting Asia, Europe and North America [6]–[10]. This connection is only available over a few months due to the comprehensive influence of various special geographical environmental factors: complicated natural environment, densely distributed islands and icebergs as well as the lack of the shipping infrastructure north of the Arctic Circle. Sea ice is one of the mostimportant natural factors, which restricts the navigation in the Arctic Passage. The detection of sea ice distribution detection in the Arctic Ocean based on FengYun-3 (FY-3) satellite data can provide reliable basic data and scientific evidence, which is of great significance for polar strategy.

The application of remote sensing technology has made sea ice detection possible. Some researchers have used optical remote sensing data to study the sea ice distribution. For example, Zhang *et al.* [11] used the spectral unmixing method for extracting sea ice concentration using two neural

networks. Su *et al.* [12], [13] extracted sea ice extent using a ratio-threshold segmentation method. Zhang *et al.* [14] proposed the sea ice extraction method using the 0.86 μm and 1.24 μm wave bands of MODIS based on the Normalized Difference Snow Index (NDSI). Zhang *et al.* [15] proposed the inversion algorithm based on the Classification and Regression Tree (CART) to retrieve sea ice from MODIS images (from 2009 to 2012) in the Bohai Sea. However, Arctic cloud cover is a limiting factor for detecting sea ice distribution in mid-summer [16], [17]. Simpson and Keller [18] proposed the combination of Wiener filtering techniques and the fuzzy logic classification method to segment clouds from sea ice and a cloud-free ocean. McIntire and Simpson [19] used a combination of feed-forward neural networks and 1.6 μm data from the FY-1C satellite to classify sea ice, clouds, and ocean/leads. Shen *et al.* [20] proposed the uneven illumination correction algorithm to remove the effect of thin clouds and restore ground information of the optical remote sensing image.

At present, the general method that removes interferences caused by clouds in optical remote sensing images is a filtering approach, but the process is complicated and time-consuming, and some information is lost. In the range of 1-1.6 μm, the reflectances of ice and water decrease and the reflectance of clouds gradually increases as wavelengths increase; cloud reflectance are much higher than that of ice and water in the near-infrared range. Thus, the discrimination condition for identifying clouds is obtained, and on the basis of this difference, regions with the thin clouds can be extracted. The classification threshold of sea water and sea ice in the cloudless regions is determined using the Otsu algorithm, and the sea ice distribution in the thin cloud regions is obtained using the influential factor iteration method. Finally, the sea ice distribution can be obtained based on the sea ice distribution in the cloud-covered and cloudless regions added together.

II. STUDY AREA AND DATA

The critical regions containing Baffin Bay and Davis Strait are selected as the study area, located between 64°-72°N and 49°-69°W. This region lies within the Northwest Passages, and is at the confluence of the West Greenland Current and Labrador Current. Therefore, the detection of the sea ice distribution in this region can indirectly effect ship navigation to parts of Greenland, and the study area can be served as the basic data for the study of climate changes in polar regions.

FY-3 satellites are sun-synchronous polar-orbiting environmental meteorological satellites with an orbit altitude of about 830 km. There are 11 instruments on FY-3, including three sounding instruments, two ozone instruments, two earth radiation budget instruments, three imaging remote sensors, and one space environment monitoring unit. MERSI is a spectral imaging sensor with medium resolution. The first MERSI was launched on May 27, 2008, on board the FY-3A satellite [21]. It is similar to the MODIS on board the Earth Observing System satellite series, except that it does not

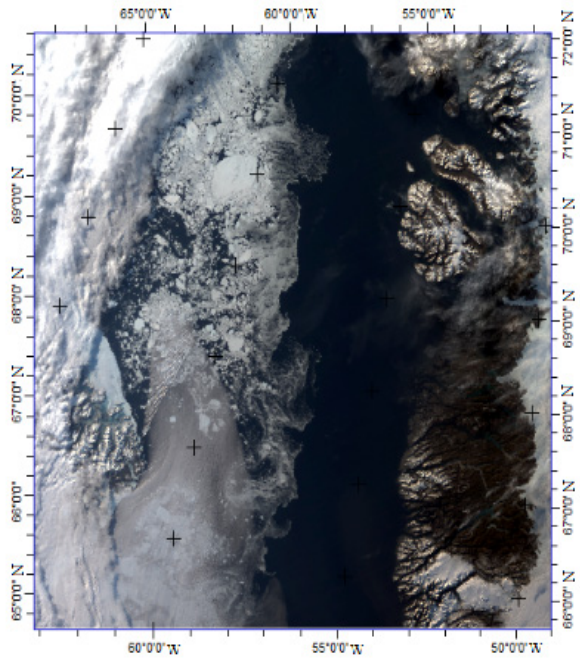

FIGURE 1. Original band1 gray image.

carry the mid-infrared channels. MERSI has 20 channels that are primarily located in the visible and the near-infrared spectral regions. Five MERSI channels (four visible and one thermal infrared) have a spatial resolution of 250 m, which can be used to create high-resolution earth imagery in natural color during the day and high-resolution thermal infrared imagery at night. The remaining MERSI channels have a spatial resolution of 1 km [21]. MERSI products record land surface reflectance, high-resolution vegetation index, land-cover types, ocean color, aerosols, and condensable atmospheric water.

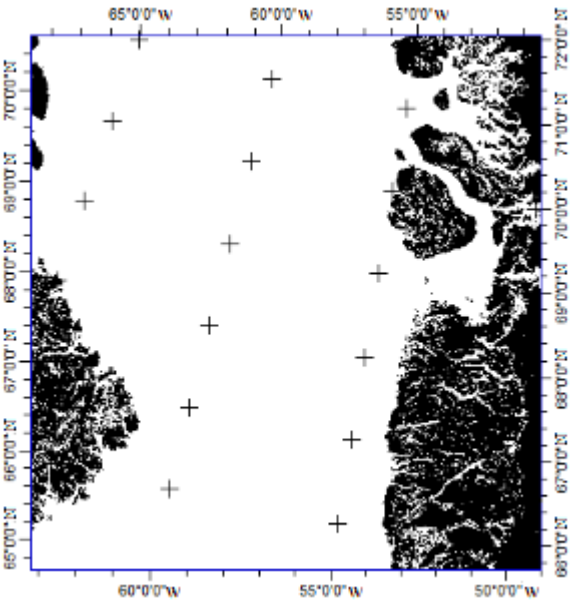

FIGURE 2. Land masking.

MERSI data from the FY-3 satellite are calibrated using the polynomial method, and pixel coordinates are obtained by projection transformation. The image of band 1 is show in Fig. 1. Land masking results are shown in Fig. 2, where the black area is land. The black crosses in Fig. 2 indicate latitude and longitude intersections.

III. THEORY AND METHOD

A. SPECTRAL CHARCTERISTIC ANALYS

The spectral characteristics of ground objects are the basis for remote sensing inversion; spectral characteristic curves of different objects mainly reflect their electromagnetic reflection or emission. The reflection characteristics of sea ice in the visible and near-infrared are important characteristics for sea ice identification. According to statistical analysis of the MODIS airborne simulator (Fig. 3) [22], the following observations are made [16], [22]–[25]:

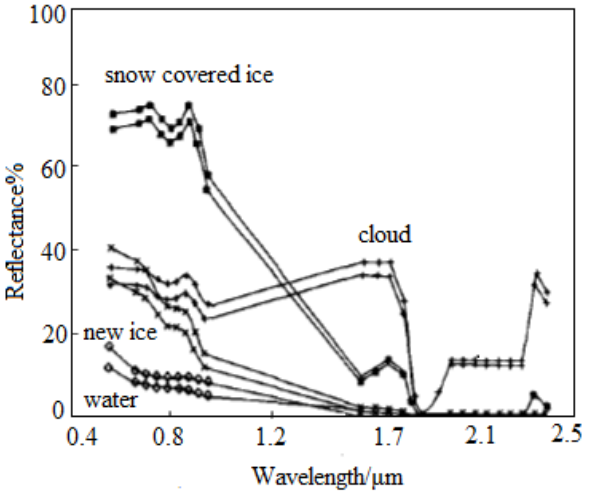

FIGURE 3. Reflectance curves for ice, clouds, water [21].

1) The reflectances of ice, new ice and clouds are higher than that of water in the visible spectral range.

2) The reflectances of water and new ice decrease gradually with the increase in wavelength in the visible and near-infrared spectral range.

3) Reflectance changes of ice and clouds are relatively small in the 0.5-0.7 μm range.

4) Reflectances of ice, new ice and water gradually decrease and reflectances of clouds gradually increases in the 1-1.6 μm range.

B. IDENTIFICATION OF THIN CLOUDS

According to the spectral characteristics of ice, clouds and water, regions with clouds are identified, and regions with thin clouds are subsequently extracted. For cloud extraction, most methods use the Normalized Difference Snow Index (NDSI) for distinguishing ice and clouds. However, the reflectances of ice covered with snow are larger as well in the vicinity of 1.6 μm. Because snow covered ice is common in polar regions, this method cannot accurately identify cloud regions. Through the analysis of spectral characteristics of ice, clouds and water, we propose a discrimination condition for cloud regions according to the changing trend of the reflectance curve. In particular, in the 1-1.6 μm range, there is a difference between the reflectances of clouds and the reflectances of ice, new ice and water. The center wavelength for band 6 is 1.64 μm and the center wavelength for band 20 is 1.03 μm for FY-3 MERSI data. The ratio of band 6 to band 20 for the area covered by clouds is greater than 1, and that of ice and water is less than 1. The ratio for snow covered ice is also greater than 1 in the range of about 1.6 μm, the only condition that does not accurately extract clouds. Reflectances of clouds are much higher than that of snow covered sea ice in the near-infrared band based on the reflectance characteristics of ice, clouds and water. The center wavelength of band 7 is 2.13μm for FY-3 MERSI data in the near-infrared band, and the appropriate threshold th_1 (Otsu threshold) is chosen as another discriminating factor for identifying clouds. The value is taken as 0.13.

The restrictions on the above two conditions can accurately identify clouds. The discriminant for identifying clouds is:

$$\begin{cases} \rho_6/\rho_{20} > 1 \\ \rho_7 > th_1 \end{cases} \tag{1}$$

where, ρ_6, ρ_{20}, and ρ_7 correspond to the reflectances of band 6, band 20, and band 7 for FY-3MERSI data, and th_1 is the classification threshold. According to the empirical formula for atmospheric precipitation, water vapor retrieval is incorporated [22]. According to the difference in water vapor retrieval results, thin clouds are identified. The water vapor retrieval formula is as follows:

$$\mathrm{W} = \left[\frac{\alpha - \ln T_w}{\beta}\right]^2 \tag{2}$$

$$\mathrm{T_w} = (\rho_{18}/\rho_{16}) = \exp\left(\alpha - \beta\sqrt{w}\right) \tag{3}$$

where, w is atmospheric precipitation, T_w is water vapor transmission rate, ρ_{16} and ρ_{18} are reflectances of band 16 and band 18 for FY-3 MERSI data.

Because the study area is in the polar regions, and ground objects covered with clouds are sea water, or bare rocks, $\alpha = 0.02$, $\beta = 0.651$. As the atmospheric precipitation from thick clouds is less than that from thin clouds, the discriminant for extracting thin clouds is:

$$\mathrm{W}_1 > th_3 \tag{4}$$

where, W_1 is the calculated result for atmospheric precipitation in all cloud regions, th_3 is the threshold set by the characteristic that thin cloud precipitation occurs at higher altitude than that of thick clouds.

The data contained in this paper all satisfy equation (4), that is, all interferences are caused by thin clouds. In order to verify the optimality of the selected threshold in the cloud regions, we obtain two-dimensional scatter plots, as shown in Fig. 4; the Y-axis is the image in band 6, and the X-axis is

the image in band 20. According to (1) and the correlative theories, the upper left of Fig. 4 contains the pixels with clouds, and the slope of the straight line is the selected optimal threshold.

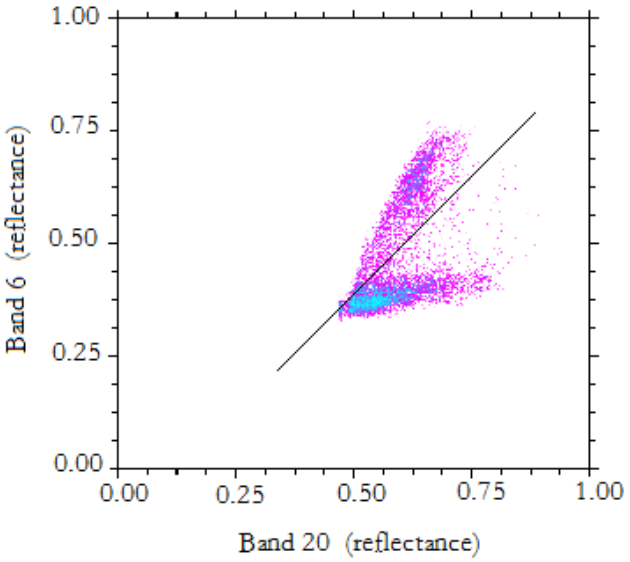

FIGURE 4. Two-dimensional scatter plots obtained from band 6 and band 20.

C. INFLUENTIAL FACTOUR ITERATION METHOD

Clouds affect the quality of remote sensing images, and thick clouds may make remote sensing data unusable. However, information from thin cloud regions in remote sensing images includes both clouds and ground objects. In order to effectively utilize remote sensing data, the influential factor iteration method is proposed to provide secondary classification of ground objects under thin cloud cover.

The core concept of the influential factor iteration method is to correct the reflectances of ground objects affected by clouds, that is, using the following mathematical model:

$$\mathrm{Y} = k\mathrm{X} \tag{5}$$

where, Y is the reflectances of ground objects affected by clouds, X is the reflectances of the same ground objects unaffected by clouds, k is the influential factor of the ground objects due to clouds. The existence of clouds will weaken the reflectances of ground objects, so the range in k is 0-1. Thicker clouds result in an influential factor close to 0, and thinner clouds have an influential factor closer to 1.

The value of the influence factor k is determined by the following method. First, in the image after thin cloud recognition, an adjacent large dark area (open water) part of the cloud pixel is selected and recorded as sample W1. The pixels in sample W1 are considered thin cloud covered sea water. Then, a large number of dark hued area cloud-free parts of the pixel are selected and recorded as sample W2. The pixels in sample W2 are considered thin cloud-covered sea water. Similarly, there are cloud pixels adjacent to the large bright hue area (adjacent to the land ice shelf area), denoted as sample I1, and the pixels in sample I1 are considered thin cloud-covered sea ice pixels. A large part of the bright colored area is selected from cloud-free part of the pixel, recorded as I2, and sample I2 is considered to be thin cloud-covered sea ice pixels. Because the Arctic regions have a relatively simple climate and environment other interferences are weak. In the study area, the influence of thin clouds on the reflectance of the underlying surface is basically the same, that is, the effect of sea ice and sea water is the same, because the study area is small and cloud thickness can be considered uniform. The value of each pixel in sample W1 is compared with W2, and the result obtained is a set of data KW. Similarly, the value of each pixel in sample I1 is compared with I2, and the results are written as a set of data KI. The mean value of each element in the set KW is the effect of thin cloud cover on each sea water pixel. The mean value of each element in the set KI is the effect of thin cloud cover on each ice pixel. The mean value of all elements of the sets KW and KI are treated as the total mean value. This obtained mean value of the image factor k produced by thin clouds in the study area. The value of k taken here is 0.95.

The discriminant of the cloudless classification threshold for sea ice and sea water is obtained through analysis of the reflectance curve as follows:

$$\begin{cases} \rho_1/\rho_2 > th_4 \\ \rho_4/\rho_3 > th_5 \end{cases} \tag{6}$$

The cloudless classification threshold for sea ice and sea water is revised through the influential factor iteration method to identify sea water as follows:

$$\begin{cases} \rho_1/\rho_2 > th_4 \times k \\ \rho_4/\rho_3 > th_5 \times k \end{cases} \tag{7}$$

where, ρ_1, ρ_2, ρ_3 and ρ_4 correspond to the reflectances of band 1, band 2, band 3 and band 4 for FY-3 MERSI data, respectively. th_4, th_5 are the classification thresholds, and k is the influential factor of the ground objects due to the influence of clouds. The pixel as shown for (6) is considered the sea water pixel in the cloud regions.

In order to verify the optimality of the selected threshold for identifying sea water, we obtain two-dimensional scatter plots as shown in Fig. 5; the Y-axis is the image from band 1, and the X-axis is the image from band 2. According to (6) and the correlative theories, the upper left of Fig. 5 is sea water, and the slope of the straight line is the selected optimal threshold.

D. DETECTION PROCESS OF SET ICE DISTRIBUTION

1) IDENTIFY THIN CLOUDS

Equation (1) is used as the criterion identifying clouds. Then, an empirical formula for atmospheric precipitation is introduced to run the water vapor retrievals. Thin clouds are extracted from the clouds according to the results of the water vapor retrievals.

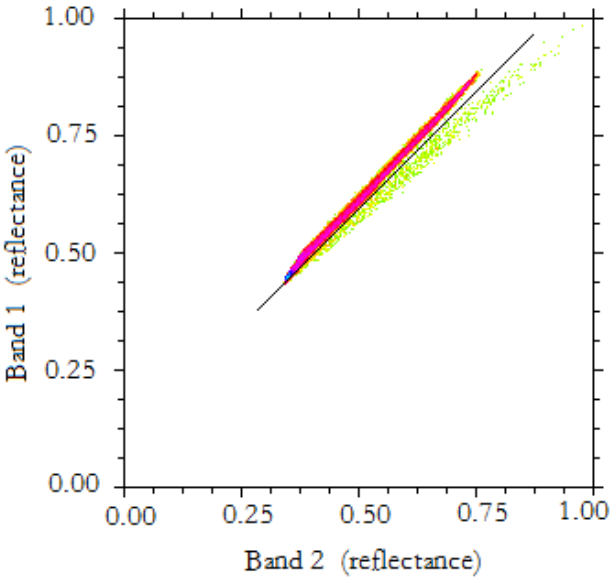

FIGURE 5. Two-dimensional scatter plots obtained from band 1 and band 2.

2) IDENTIFY SEA WATER IN THE CLOUDLESS REGIONS

The sea ice reflectance change is smaller, while the sea water reflectance change is larger in the 0.4-0.9 μm range. Therefore, the ratio of band 1 (center wavelength 0.47 μm) and band 2 (center wavelength 0.55 μm) for sea ice is less than 1, and that of the sea water is greater than 1. Therefore, the value of th_4 is chosen as 1.12. In order to distinguish sea water more accurately, the 0.5-0.9 μm wavelengths are used; within this range, the reflectances of sea water trend are small. Band 4 (center wavelength 0.865 μm) and band 3 (center wavelength 0.65 μm) are compared. The sea water value in the resulting ratio image is greater than the value of new ice, and both are less than 1, but the sea water value is closer to 1. Therefore, the appropriate threshold th_5 is selected to obtain the discriminant for sea water identification in the cloudless regions, that is, the pixel satisfying equation (6) can be determined from the sea-free water pixel without clouds. The method for determining th_5 also uses the largest interclass variance method, where the value is 0.96.

3) IDENTIFY SEA WATER IN THE CLOUD REGIONS

Thus far, land, clouds and sea water from cloudless regions have been identified. The threshold identifying sea water in cloud-covered regions is modified by the influential factor iteration method combined with the Otsu threshold. That is, equation (7) is used as the criteria for identifying sea water in cloud-covered regions.

4) EXTRACT SEA ICE DISTRIBUTION

Sea ice distribution information can be obtained in the cloudless regions and cloud regions through the above steps.

IV. RESULTS AND DISCUSSION

Based on (1-4), the ratio images of band 6 and band 20 are processed to obtain the thin cloud results as shown in Fig. 6, where black indicates thin cloud cover and white indicates other ground objects.

FIGURE 6. Extracting thin clouds.

The values th_4 and th_5 in (6) are obtained from the Otsu method, and then the sea water distribution for the cloudless regions is obtained, as shown in Fig. 7; white indicates sea water in the cloudless regions, black is the sea ice in the cloudless regions, and land and ground objects covered with thin clouds.

FIGURE 7. Sea water distribution of the cloudless regions.

On the basis of (6), the classification threshold for sea ice and sea water under thin clouds are obtained by modifying the classification threshold for sea ice and sea water in the cloudless regions using the influential factor iteration method. The final sea water distribution is shown in Fig. 8 under the condition of (7); white is sea water under the thin clouds, black is sea ice covered with the thin clouds as well as the ground objects in cloudless regions.

The sea ice distribution in the cloudless regions is shown in Fig. 9 based on the cloudless regions sea water distribution. The sea ice distribution under thin clouds is shown in Fig. 10 based on the sea water distribution under

FIGURE 8. Final sea water distribution under thin clouds.

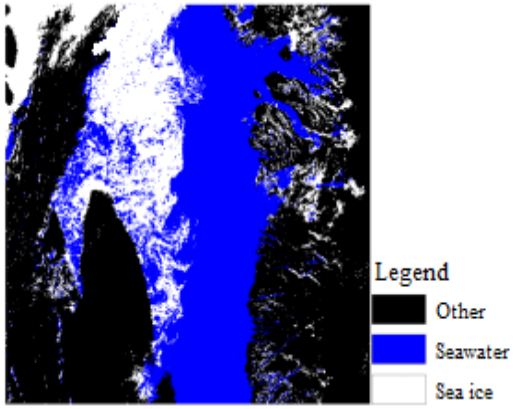

FIGURE 9. Sea ice distribution of cloudless regions.

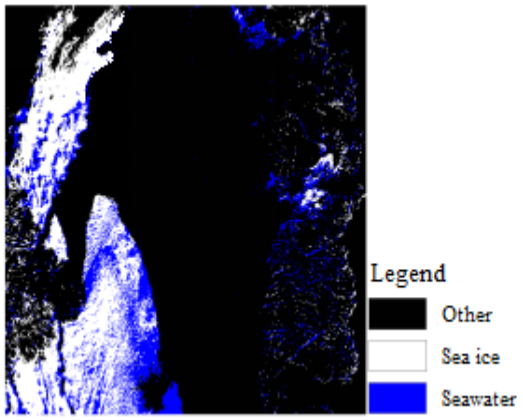

FIGURE 10. Sea ice distribution under thin clouds.

thin clouds. The final sea ice distribution in the entire study area can be obtained as shown in Fig. 11 (Fig. 9 and Fig. 10 are superimposed, and then the results are re-sampled to 4 km). Fig. 12 is the sea ice distribution (spatial resolution 4 km) of NSIDC, which is obtained from DMSP SSM/I satellite data. Through the comparison of Fig. 11 and Fig. 12 we find that the sea ice distribution obtained using FY-3 MERSI data is consistent with the sea ice distribution

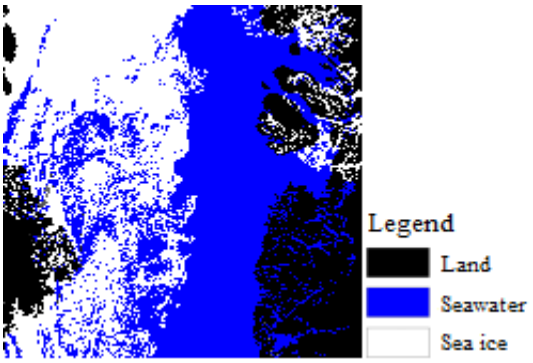

FIGURE 11. Final sea ice distribution.

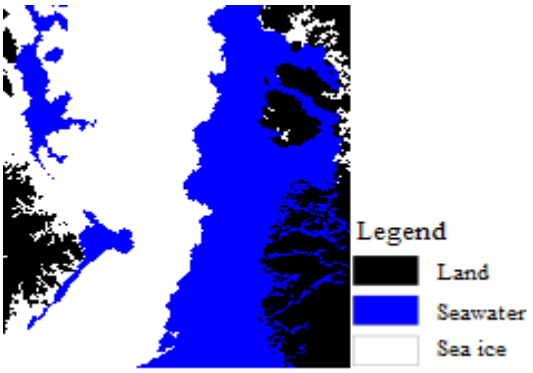

FIGURE 12. Sea ice distribution from NSIDC.

from NSIDC in the melt edge lines. But there are some differences between the two results. It can be seen that our results have more detailed and accurate sea ice distribution including floating ice and drift ice by comparing with the original color image (Fig. 1). In comparison, results obtained from NSIDC are smoother and the overall information of the sea ice distribution.

There are differences in the upper right part of the two results. Among them, there are only a small amount of sea water pixels in the upper part of Fig. 11, and there is a large area of sea water pixels in the upper part of Fig. 12. The reasons for these differences may be as follows: (1) Although FY-3 satellite data and DMSP satellite data are the same day, the transit time is different. (2) The differences are likely to be caused by the wind. The study area is at the junction (Baffin Bay) of the warm currents of the North Pacific and the cold currents of the Arctic Ocean. Therefore, even if there is brief difference in time between the two satellites, the wind may cause some differences in the sea ice distribution. (3) The differences are mainly sits at the junction of the land and the sea. Studies have shown that it can cause some errors in the inversion of sea ice concentration based on remote sensing data at the junction of the land and the sea.

However, the proposed method is still limited, which is only applicable to the identification of sea ice influenced by thin clouds in the small area. We will expand the applicable range of the algorithm in future, and we will study the Arctic Ocean using the data with the different cloud thickness at

the same time. Theoretical basis and implementation steps are as follows: First of all, identify the type and thickness of all clouds according to the water content and the height of the clouds. Secondly, the different types of clouds and different thickness of clouds are studied separately to obtain their reflectance parameters. Finally, the two parameters are combined by mathematical idea to build a model. The difficulties are how to optimize the combination of the two parameters in a mathematical way. This will be the next efforts and overcome the difficulties.

V. CONCLUSION

Based on the differences in reflectance of sea ice, water and clouds in the visible and near-infrared, FY-3 MERSI data is preprocessed. The study area is divided into the cloudless regions and cloud-covered regions through a binary tree classification. First, a two-band ratio (the ratio of band 6 to band 20) and single wave band (band 7) thresholds are selected as the criteria identifying the basic cloud regions. Then the empirical formula for atmospheric precipitation is introduced to extract thin clouds from the basic cloud regions. Due to the impact of clouds on the reflectance, there are the different thresholds in the cloudless regions and cloud-covered regions, so the influential factor iteration method was used to modify the threshold in the thin cloud regions, and then get the sea ice distribution in the thin cloud regions. Finally, the sea ice distribution is obtained in the critical regions containing Baffin Bay and Davis Strait. In conclusion, the following conclusions can be drawn:

(1) On the premise that the thin clouds are not removed, the proposed influential factor iteration method can identify sea ice. The real information of the original data is preserved effectively, and the accuracy of sea ice detection is improved. To some extent, it also reduces the workload of the sea ice retrieval process.

(2) Compared with the results from NSIDC, the sea ice distribution obtained using FY-3 MERSI data is basically the same with the sea ice distribution from NSIDC, and our results have more detailed distribution of floating ice and drift ice. That is, in terms of reducing the influence of thin clouds, the proposed sea ice detection method is feasible.

REFERENCES

[1] W. Shi and M. Wang, "Sea ice properties in the Bohai Sea measured by MODIS-Aqua: 1. Satellite algorithm development," *J. Marine Syst.*, vol. 95, pp. 32–40, Jul. 2012.

[2] A. Letterly, J. Key, and Y. H. Liu, "The influence of winter cloud on summer sea ice in the Arctic, 1983–2013," *J. Geophys. Res., Atmos.*, vol. 121, no. 5, pp. 2178–2187, 2016.

[3] M. C. Serreze and J. A. Francis, "The Arctic amplification debate," *Climatic Change*, vol. 76, pp. 241–264, Jun. 2006.

[4] P. U. Clark, R. B. Alley, and D. Pollard, "Northern Hemisphere ice-sheet influences on global climate change," *Science*, vol. 286, no. 5442, pp. 1104–1111, 1999.

[5] X. Miao, H. Xie, S. F. Ackley, and S. Zheng, "Object-based arctic sea ice ridge detection from high-spatial-resolution imagery," *IEEE Geosci. Remote Sens. Lett.*, vol. 13, no. 6, pp. 787–791, Jun. 2016.

[6] J. C. Comiso, "A rapidly declining perennial sea ice cover in the Arctic," *Geophys. Res. Lett.*, vol. 29, no. 20, pp. 17-1–17-4, 1956, doi: 10.1029/2002GL015650.

[7] J. C. Comiso, "Abrupt decline in the Arctic winter sea ice cover," *Geophys. Res. Lett.*, vol. 33, no. 18, p. L18504, 2006, doi: 10.1029/2006GL027341.

[8] W. N. Meier, J. Stroeve, and F. Fetterer, "Whither arctic sea ice? A clear signal of decline regionally, seasonally and extending beyond the satellite record," *Ann. Glaciol.*, vol. 46, no. 1, pp. 428–434, 2007.

[9] M. C. Serreze *et al.*, "A record minimum arctic sea ice extent and area in 2002," *Geophys. Res. Lett.*, vol. 30, no. 3, p. 1110, 2003, doi: 10.1029/2002GL016406.

[10] J. Stroeve, M. Holland, W. Meier, T. Scambos, and M. Serreze, "Arctic sea ice decline: Faster than forecast," *Geophys. Res. Lett.*, vol. 34, no. 9, p. L09501, 2007, doi: 10.1029/2007GL029703.

[11] D. Zhang, C. Ke, B. Sun, R. Lei, and X. Tang, "Extraction of sea ice concentration based on spectral unmixing method," *J. Appl. Remote Sens.*, vol. 5, no. 1, p. 053552, 2011.

[12] H. Su and Y. Wang, "Using MODIS data to estimate sea ice thickness in the Bohai Sea (China) in the 2009–2010 winter," *J. Geophys. Res., Oceans*, vol. 117, no. C10, p. C10018, 2012, doi: 10.1029/2012JC008251.

[13] H. Su, Y. Wang, and J. Yang, "Monitoring the spatiotemporal evolution of sea ice in the Bohai Sea in the 2009–2010 winter combining MODIS and meteorological data," *Estuaries Coasts*, vol. 35, no. 1, pp. 281–291, 2011.

[14] X. Zhang, C. Zhou, and J. An, "Monitoring of antarctic sea ice based on the multichannel MODIS data," *Geomatics Inf. Sci. Wuhan Univ.*, vol. 39, no. 10, pp. 1194–1198, 2014.

[15] N. Zhang, Y. Wu, and Q. Zhang, "Detection of sea ice in sediment laden water using MODIS in the Bohai Sea: A CART decision tree method," *Int. J. Remote Sens.*, vol. 36, no. 6, pp. 1661–1674, 2015.

[16] T. C. Grenfell and D.K. Perovich, "Spectral albedos of sea ice and incident solar irradiance in the southern Beaufort Sea," *J. Geophys. Res., Oceans*, vol. 89, no. C3, pp. 3573–3580, 1984.

[17] D. K. Hall *et al.*, "Algorithm Theoretical Basis Document (ATBD) for the MODIS snow and sea ice-mapping algorithms," NASA GSFC, Tech. Rep., 2001. [Online]. Available: http://modis.gsfc.nasa.gov/data/atbd/atbd_mod10.pdf

[18] J. J. Simpson and R. H. Keller, "An improved fuzzy logic segmentation of sea ice, clouds, and ocean in remotely sensed Arctic imagery," *Remote Sens. Environ.*, vol. 54, no. 3, pp. 290–312, 1995.

[19] T. J. McIntire and J. J. Simpson, "Arctic sea ice, cloud, water, and lead classification using neural networks and 1.6-μm data," *IEEE Trans. Geosci. Remote Sens.*, vol. 40, no. 9, pp. 1956–1972, Sep. 2002.

[20] X. Shen, Q. Li, Y. Tian, and L. Shen, "An uneven illumination correction algorithm for optical remote sensing images covered with thin clouds," *Remote Sens.*, vol. 7, no. 9, pp. 11848–11862, 2015.

[21] X. Hu *et al.*, "Calibration for the solar reflective bands of medium resolution spectral imager onboard FY-3A," *IEEE Trans. Geosci. Remote Sens.*, vol. 50, no. 12, pp. 4915–4928, Dec. 2012.

[22] G. A. Riggs, D. K. Hall, and S. A. Aakerman, "Sea ice extent and classification mapping with the moderate resolution imaging spectroradiometer airborne simulator," *Remote Sens. Environ.*, vol. 68, no. 2, pp. 152–163, 1999.

[23] Y. J. Kaufman and B.-B. Gao, "Remote sensing of water vapor in the near IR from EOS/MODIS," *IEEE Trans. Geosci. Remote Sens.*, vol. 30, no. 5, pp. 871–884, Sep. 1992.

[24] D. K. Perovich, "Seasonal changes in sea ice optical properties during fall freeze-up," *Cold Regions Sci. Technol.*, vol. 19, no. 3, pp. 261–273, 1991.

[25] D. K. Perovich, C. S. Roesler, and W. S. Pegau, "Variability in Arctic sea ice optical properties," *J. Geophys. Res., Oceans*, vol. 103, no. C1, pp. 1193–1208, 1998.

XING-DONG WANG was born in Shanxi, China, in 1982. He received the Ph.D. degree in resources and environmental remote sensing from Central South University, China, in 2013. He was a Post-Doctoral Student with the Institute of Remote Sensing and Digital Earth, Chinese Academy of Sciences, China, from 2014 to 2017. His current research interests are in the ice sheet and sea ice detection based on the optical and microwave remote sensing data.

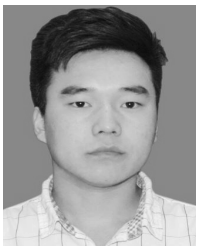

ZHAN-KAI WU was born in Henan, China, in 1993. He received the bachelor's degree in space information and engineering technology from the Henan University of Technology, Zhengzhou, China, in 2017, and the master's degree in cartography and geographical information system from the College of Information Science and Engineering, Henan University of Technology in 2017. His current research interests are in the sea ice distribution detection based on the optical remote sensing data.

CHENG WANG was born in Hunan, China, in 1975. He received the B.S degree in remote sensing and GIS from Nanjing Normal University, China, in 2003, and the Ph.D. degree in laser radar remote sensing from Louis Pasteur University, France, in 2005. He was a Research Assistant with Idaho State University, USA, from 2007 to 2009. His current research interests are in laser radar remote sensing, hyperspectral remote sensing, and global change.

XIN-WU LI was born in Sichuan, China, in 1973. He received the B.S degree in applied geophysics from the China University of Geosciences, Beijing, China, in 1999, and the Ph.D. degree in cartography and geographical information system from the University of Chinese Academy of Sciences, China, in 2002. His current research interests are in environmental radar remote sensing, global environmental change and remote sensing, polar environment and remote sensing, ecological environment remote sensing, and urban environment remote sensing.

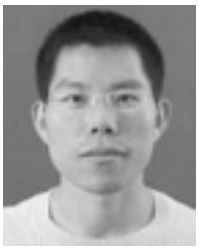

XIN-GUANG LI was born in Henan, China, in 1977. He received the B.S degree in geographic information system and the Ph.D. degree in cartography and geographic information engineering from Wuhan University, China, in 2007 and 2012, respectively. His current research interests are in spatial information services, data mining, and informatics.

YU-BAO QIU was born in Jiangxi, China, in 1978. He received the Ph.D. degree in cartography and geographical information system from the Chinese Academy of Sciences, China, in 2008. He was with the Helsinki University of Technology, Finland, from 2007 to 2008, as a Research Scientist involved in microwave remote sensing, and the Group on Earth Observations from 2012 to 2015, as a Science and Technology Officer involved in water and the ecosystem. His current research interests are remote sensing of snow and ice in high mountain and cold regions.